Earthquake Resilience of Spatially Distributed Building Clusters: Methodology and Application

Silvestre Chan Esquivel¹; Yiming Jia, A.M.ASCE²; and Mehrdad Sasani, F.ASCE³

ABSTRACT

Interest in earthquake resilience has increased in recent years, and the use of building cluster performance objectives has been shown to be an effective method for evaluating the resilience of built environment. A building cluster is a portfolio of buildings that share the same role in a community; its performance objectives are defined by considering earthquake scenarios, hazard levels, and individual building performance. The methodology presented in this paper employs performance-based assessments to estimate the probability of achieving building cluster performance objectives immediately following a seismic event. It can be used to assess the immediate postearthquake community resilience in five steps: 1) hazard analysis, 2) conditional assessment of individual building performance, 3) conditional assessment of building cluster performance, 4) building cluster performance assessment by aggregation, and 5) earthquake resilience assessment of building clusters considering all hazard levels of interest. The design and extreme hazard levels are formulated using ground motion records selected based on the conditional spectra considering characteristics of earthquake scenarios and spatial correlation. Three performance objectives are defined for both individual buildings and building clusters: functionality, safe and usable during repair, and collapse prevention. Two engineering demand parameters - the maximum transient and the permanent interstory drift indices – are used to estimate individual building performance. The probability of achieving building cluster performance objective is calculated using the total probability theorem. The application of the proposed methodology is demonstrated using two clusters of reinforced concrete buildings, corresponding to ASCE 7 Risk Category II and IV structures, in San Francisco, CA.

¹ Ph.D. Department of Civil and Environmental Engineering, Northeastern University, Boston, MA. Email: chanesquivel.s@northeastern.edu

² Ph.D. candidate, Department of Civil and Environmental Engineering, Northeastern University, Boston, MA. Email: <u>jia.yim@northeastern.edu</u>

³ Professor, Department of Civil and Environmental Engineering, Northeastern University, Boston, MA, Email: sasani@neu.edu, Tel: 617-373-5222

Keywords: Building clusters; performance objectives; earthquake resilience; nonlinear dynamic analysis; building performance; aggregation; conditional spectra; spatial correlation

INTRODUCTION

Research on community resilience has expanded substantially in recent years. Several works have been dedicated to establishing general guidelines (Bruneau et al., 2003), metrics to measure (Bruneau et al., 2007), and performance goals related to community resilience (Spur, 2008; WSEMC, 2012; OSSPAC, 2013). Seismic is the most studied hazard when evaluating resilience at the community level (Koliou et al., 2020). An early attempt to define earthquake resilience goals was presented in Spur (2008), which developed illustrative goals for buildings in San Francisco, CA, for a 7.2magnitude seismic event. NIST (2015) refined the concept of performance objectives for individual buildings from Spur (2008) to develop performance objectives for building clusters, where a building cluster is comprised of buildings with the same role in a community (e.g., residential housing, essential facilities). The performance objectives in NIST (2016) were developed based on four components: hazard level, building performance level, recovery phase, and threshold value related to the desired performance level of the cluster. This refinement effort resulted in a tool that decisionmakers can use to assess a community's current state of resilience. However, due to the limited funds, the anticipated performance of building cluster in NIST (2016) was determined by expert judgment, and the accuracy would likely improve, as better tools became available (NIST 2016). Mieler et al. (2015) proposed a conceptual framework to evaluate the effect of individual building performance on community level resilience goals. In Mieler et al. (2015), the resilience goals were expressed in terms of the risk of undesirable socio-economic outcomes (e.g., outmigration) due to the loss of vital community functions, and evaluated using a performance-based assessment methodology for either a hazard event or over a time period. It is worth noting that Mieler et al. (2015) subdivided these vital community functions into contributions of building clusters but did not account for correlations among building performances.

Despite the established frameworks of resilience evaluation, there are some knowledge gaps that need to be addressed before implementing resilience-based assessment at the community level (Cimellaro et al., 2010; Koliou et al., 2020). First, as the foundation of community resilience evaluation, the individual building performance needs to be reasonably assessed. Several models have been developed to probabilistically evaluate performance metrics at the individual building level across

time by considering post-earthquake building performance and recovery paths or trajectories to the full functional recovery (Burton et al., 2016; Lin and Wang, 2017; FEMA, 2018a; Terzic et al., 2021; Cook et al., 2022; Molina Hutt at al., 2022). These developed models are usually conditioned on either a given earthquake scenario or hazard level. However, a community may have several earthquake scenarios and/or hazard levels. As the second knowledge gap, the seismic hazard analysis is usually developed for individual sites rather than for a region (Bocchini et al., 2016; Koliou et al., 2020). Even recent works bridge this gap by assessing functionality across a community conditioned on a given earthquake scenario (e.g., Lin et al., 2016; Nozhati et al., 2019), at the community level, one earthquake scenario might have a different contribution/importance to the hazard level of a site. It means that additional works are needed, such as aggregating the assessments of several earthquake scenarios into a community level assessment for a given hazard level (e.g., Burton et al., 2016; Lin and Wang, 2017). Considering building clusters located at different sites of a community, the third knowledge gap is that the spatial correlations between ground motion (GM) intensity measure at every location need to be well estimated (e.g., Goda and Hong, 2008; Jayaram and Baker, 2009; Markhvida et al., 2018; Heresi and Miranda, 2019) and embedded in the community resilience assessment (Heresi and Miranda 2023).

Recently, some frameworks for community-scale resilience assessment have been proposed. Burton et al. (2016) extended existing performance-based earthquake engineering (PBEE) frameworks to incorporate probabilistic building performance limit states in the assessment of community resilience – post-earthquake functionality and recovery path. Lin and Wang (2017) developed a simulation-based building portfolio recovery model to predict the functionality recovery time and recovery trajectory of a community-building portfolio following natural hazard events. Heresi and Miranda (2023) formalized a mathematical extension based on the PBEE framework (Deierlein et al., 2003; Moehle and Deierlein, 2004) to evaluate the number of damaged structures and total economic loss for a community. However, these frameworks lack mathematical quantification for the propagation of correlation among engineering demand parameters (EDPs) and do not focus on the short-term recovery phase earthquake resilience. In addition, in the context of evaluating community resilience, stakeholders may be more interested in the functionality of a certain type of building clusters, rather than the structural and nonstructural damages.

The methodology proposed in this paper expands the PBEE framework (Deierlein et al., 2003; Moehle and Deierlein, 2004) in order to assess building cluster performance objectives (BCPOs) at a community level immediately after a seismic event. More specifically, compared with the PBEE framework, which is developed for individual buildings, the proposed methodology can assess building performance of spatially distributed buildings conditioned on a given hazard-level intensity measure. The four basic steps of the PBEE framework, i.e., hazard analysis, structural analysis, damage assessment, and loss assessment, are employed in this methodology, with the following main extensions to achieve the community-level performance assessment. The first extension is that the hazard analysis is adapted for building clusters by including cross and spatial correlations of a seismic intensity measure using conditional spectra (Baker, 2011; Lin et al., 2013; Lin and Baker, 2015), which can provide guidance for GM selection at a community level. Furthermore, extreme (deterministic and probabilistic) and design hazard levels are defined and evaluated. As the second extension, a joint probability model, which can account for the correlation among EDPs (e.g., the maximum transient and the permanent interstory drift indices), is proposed to estimate the probability of failure of individual building conditioned on a given hazard level. This indicates that the correlation among EDPs of spatially distributed buildings is considered in the damage assessment step. As the third extension, BCPOs are defined based on a hazard level, a target building performance, and a building cluster performance threshold value using the proposed resilience metric – usable floor area. The loss is defined as the percentage of floor area of building cluster not satisfying BCPOs, which can be quantified by aggregating the conditional assessments of individual building performance within a building cluster via the total probability theorem.

The proposed methodology focuses on the building cluster performance immediately following a seismic event (short-term recovery phase), the intermediate- and long-term recovery phases as defined in NIST (2016) are not within the scope of this paper. Therefore, the proposed methodology can be used to evaluate earthquake resilience for the short-term recovery phase.

METHODOLOGY

The proposed methodology is based on the PBEE framework (Deierlein et al., 2003; Moehle and Deierlein, 2004). The immediate post-earthquake community resilience is assessed in five steps: hazard analysis, conditional assessment of individual building performance, conditional assessment of a building cluster, building cluster performance assessment by aggregation, and earthquake

resilience assessment considering all hazard levels of interest. Community resilience is evaluated/quantified as the probability of building cluster achieving target BCPOs. Due to the spatial distribution of buildings and considering seismic hazard and site class may vary across the community of interest, the community is discretized into subareas, which are defined such that seismic hazard can be considered approximately the same in each subarea. Using subareas as opposed to individual buildings as basic analysis unit can significantly reduce the computation cost (i.e., number of nonlinear time history analyses). However, as a trade-off, the assessment accuracy using subareas is lower than the one using individual buildings. Buildings in each subarea are categorized based on their fundamental period of vibration, lateral-load-resisting system, site class, and ASCE 7 Risk Category (ASCE, 2022). The steps in this community resilience assessment methodology are elaborated in the following sections and the important variables are defined in Notation.

Hazard Analysis

The first step in this methodology is to perform hazard analysis for each subarea. Analogous to NIST (2016), two hazard levels are defined as extreme and design. The extreme hazard level is considered for both probabilistic and deterministic hazards. Because both extreme hazard levels can provide insight into how the building response, and in turn affect the building cluster performance and resilience assessment. The probabilistic extreme hazard level has a severity consistent with a mean annual frequency corresponding to a 2% probability of exceedance in 50 years from a site-specific hazard curve. The deterministic extreme hazard level is used for regions close to active faults, where the site-specific risk-targeted maximum considered earthquake (MCE_R) response spectrum is usually controlled by the deterministic MCE_R GM, i.e., the 84th percentile 5% damped spectral response acceleration in the direction of maximum horizontal response. It indicates that the deterministic extreme hazard level is consistent with the ASCE 7 multi-period MCE_R response spectrum (ASCE, 2022). The design hazard level is represented by the ASCE 7 design response spectrum (ASCE, 2022), which is computed as 2/3 of the multi-period MCE_R spectrum. The routine hazard level defined by NIST (2016) that uses lower severities is not considered in this paper.

In this methodology, the GM intensity measure, $S_{a_{RotD50}}$, is used to link the structural response and GM records. $S_{a_{RotD50}}$ is the 5% damped spectral acceleration (S_a) that represents a 50% fractile over all rotation angles of the two as-recorded horizontal components of a GM (Boore, 2010). S_a is preferred over other intensity measures (e.g., peak ground acceleration/velocity) to capture the hazard

intensity at different periods in several subareas. Since the orientation of GM to the main axes of the lateral-load-resisting system is random, $S_{a_{RotD50}}$ is selected to obtain a median response of a building cluster subject to seismic excitation.

Conditional assessment of individual building performance

Conditional spectra for spatially distributed buildings

Conditional spectra (CS) are widely used in seismic performance assessments because they are consistent with a hazard level yet do not assume that the same hazard level S_a occurs at all periods for a single GM (Baker, 2010; Lin et al., 2013; Lin and Baker, 2015). In this paper, CS are expanded to probabilistically estimate S_a at the fundamental periods of spatially distributed buildings. The conditional probability distribution of S_a over a range of periods is estimated by assuming a multivariate normal distribution among S_a at different periods (Jayaram and Baker, 2008; Lin and Baker, 2015). The CS for a given hazard level at the fundamental period, T^* , of the conditioning building are calculated using 1) an earthquake scenario to estimate the S_a probability distribution based on GM prediction equations, 2) a hazard-consistent S_a at T^* , and 3) correlation coefficients among S_a at different periods (cross-correlation) (Lin et al., 2013). The CS calculation are shown in Equations 1a to 1c, as

$$\varepsilon^* = \frac{\ln[S_a(T^*)] - \mu_{\ln Sa}(M, R^*, \boldsymbol{\theta}, T^*)}{\sigma_{\ln Sa}(M, R^*, \boldsymbol{\theta}, T^*)}$$
(1a)

$$\mu_{lnS_a(T_i)|lnS_a(T^*)} = \mu_{lnS_a}(M, R_i, \boldsymbol{\theta}, T_i) + \rho(T_i, T^*, \Delta)\sigma_{lnS_a}(M, R_i, \boldsymbol{\theta}, T_i)\varepsilon^*$$
(1b)

$$\sigma_{lnS_a(T_i)|lnS_a(T^*)} = \sigma_{lnS_a}(M, R_i, \boldsymbol{\theta}, T_i) \sqrt{1 - [\rho(T_i, T^*, \Delta))]^2}$$
 (1c)

where $\mu_{lnSa}(M, R, \boldsymbol{\theta}, T^*)$ and $\sigma_{lnSa}(M, R, \boldsymbol{\theta}, T^*)$ represent the average logarithmic mean and standard deviation of the GM prediction equations for a conditioning building with fundamental period T^* located at a distance (R) for a scenario defined by the geographic coordinates of the rupture site, a moment magnitude (M), and a rupture mechanism $(\boldsymbol{\theta})$. CS at each subarea, located at a distance R_i from the rupture site, is computed using Equations 1b and 1c for a range of periods T_i . $\rho(T_i, T^*, \Delta)$ represents the correlation on S_a between the building with period T_i and the conditioning building,

separated by a geographic distance Δ . For buildings in the same subarea, i.e. $\Delta = 0$, $\rho(T_i, T^*, \Delta)$ is equal to the cross correlation of S_a (Baker and Jayaram, 2008). For buildings in the different subareas, $\rho(T_i, T^*, \Delta)$ is equal to the multiplication of cross-correlation and the spatial correlation of S_a (Goda and Hong, 2008).

The deterministic scenario(s) used in CS computations is consistent with the fault rupture that defines MCE_R S_a intensity for the conditioning building according to ASCE 7 site-specific procedures (ASCE, 2022). For the design hazard level, ASCE 7 does not define the design spectrum based on any underlying scenarios. Therefore, we formulate the GM prediction equations' S_a probability distribution for the MCE_R with the median at each period scaled down by the ratio of 2/3 (ASCE, 2022; Joyner et al., 2021). For the probabilistic hazard level, the scenarios are determined from hazard deaggregation for the conditioning building using the Uniform Hazard Tool (USGS, 2018). Cumulatively, the considered scenarios contribute to more than 90% of the total rate of exceedance of the conditioning building's probabilistic S_a .

Ground motion selection

Sets of GM records scaled to S_a at T^* are selected to match CS and then used for nonlinear time history analysis. ASCE 7 (ASCE, 2022) permits the use of 11 GMs for each spectrum. However, based on the sensitivity study, the use of 20 GMs can accurately represent the median and logarithmic standard deviation of the CS (see Figure 7 in the application section), while maintaining a reasonable computation cost for nonlinear time history analysis. Similar observations are reported by Joyner and Sasani (2020) and Joyner et al. (2021).

Since the frequency content of GMs used in nonlinear time history analysis can influence the probability distributions of engineering demand parameters (EDPs, Baker et al., 2021), the same GM records are utilized across different hazard levels when possible. In addition, considering the pulse-type GMs have a larger damage potential than the ordinary GMs, the selection procedure accommodates a portion of the selected GM records being pulse-type (NIST, 2011; Joyner et al., 2022). The proportion of pulse-type GMs can be calculated using a given earthquake scenario and hazard level (NIST, 2011). The GM selection is carried out using a procedure similar to Baker (2011) and Baker and Lee (2018).

Individual building performance

Individual building performance is evaluated using the EDPs' probability distributions resulting from the nonlinear time history analyses for the selected GMs. To evaluate earthquake resilience, three building performance levels are selected to assess the state of the buildings' ability to satisfy their community roles following a seismic event: functionality, safe and usable during repair, and collapse prevention. These discrete building performance levels are defined using two EDPs per building – the maximum transient interstory drift index (IDI_{max}) and the permanent interstory drift index (IDI_{p}). Both EDPs are assumed to be lognormally distributed (Joyner and Sasani, 2018). Median and logarithmic standard deviation, β , of drift capacities for the building performance levels are provided in Table 1. β is assumed to be equal for both IDI_{max} and IDI_{p} , since there is not enough information on the dispersion for IDI_{p} . In Table 1, the collapse limits represent the values for reinforced concrete special moment frames (Haselton and Deierlein, 2008; Haselton et al., 2011).

Limits for functionality are determined based on the performance of nonstructural components. Risk Category II and IV buildings are assumed using typical and enhanced partitions, respectively. Typical partitions are full height and fixed below and above, and enhanced partitions are partial height and fixed below with a lateral brace above (FEMA, 2012; Araya-Letelier, 2014; Araya-Letelier et al., 2019). For $IDI_{max} = 1\%$, the expected damage for typical and enhanced partitions is moderate and slight, respectively (FEMA, 2018b). The IDI_p limit of 0.2% for functionality in both Risk Category II and IV buildings correspond to the less demanding damage state (no realignment needed due to permanent drift) defined in FEMA P-58-1 (FEMA, 2018a). β is selected as 0.3 (FEMA, 2018b).

Limits for safe and usable during repair performance shown in Table 1 are selected with consideration of the safety of both structural and nonstructural components (Spur, 2008; Lizundia and Gallagher, 2015). The safe and usable during repair capacities in Table 1 are proposed following an analysis of applicable standards (SEAOC, 1995; FEMA, 2005; FEMA, 2018b; ASCE, 2022) and based on comparisons with the damage descriptions for life safety performance in ASCE 41 (ASCE, 2017). The capacity for structural components is set as IDI_{max} = 2% (FEMA, 2004) and the limit used in design for Risk Category II buildings with an intended safety performance under design hazard (ASCE, 2022). For nonstructural components, wide crack openings and, if applicable, buckling of studs and tearing of tracks are accepted for typical and enhanced partitions. Since the associated IDI

capacities are 2.1% and 1.8% for typical and enhanced partitions, respectively (FEMA, 2018c), for simplicity, 2% is set as the capacity for nonstructural components.

While a 2% *IDI* capacity may seem large for nonstructural elements to be considered safe, larger drift capacities have been suggested in FEMA P-58-3 (FEMA, 2018b). A corresponding value can be inferred from the assumed fragility for an unsafe placard in FEMA P-58-3 (FEMA, 2018b). Using the capacity parameters for the damage state triggering an unsafe placard for special moment frames ($IDI_{max} = 5\%$ median, $\beta = 0.5$ for damage state 3 [DS3]) and the percentage of damaged components related to an unsafe placard (20% of the structural components in DS3) indicated in the fragility database of FEMA P-58-3 (FEMA, 2018b), $IDI_{max} = 3\%$ is representative of a post-earthquake unsafe placard in special moment frames. Since the damage to nonstructural components at $IDI_{max} = 3\%$ is expected to be significant, and in order to maintain consistency with similar design limits (ASCE, 2022), a median $IDI_{max} = 2\%$ is used in this paper. The IDI_p limit used in this methodology for safe and usable during repair performance corresponds to the IDI_p value for moderate damage with realignment needed from FEMA P-58-1 Table C1 (FEMA, 2018a). $\beta = 0.3$ is selected based on the average of the total dispersion shown in FEMA P-58-3 (FEMA, 2018b) for the damage states used to define the IDI_{max} capacity.

Limits for collapse prevention performance are selected based on IDI_{max} for structural components. Haselton et al. (2011) present IDI_{max} median capacities based on collapse assessments of reinforced concrete special moment frames code-conforming buildings. Based on the buildings' fundamental periods, the IDI_{max} capacities shown in Haselton et al. (2011) are adapted for the representative buildings presented in the application section (see Table 1). Since the variability in IDI_{max} and S_a near collapse are shown to be comparable considering only record-to-record variability (Haselton and Deierlein, 2008), β is set equal to 0.6 to account for the uncertainty of structural model.

The probability of failure of building i in subarea j for BP_n , $P_f(BP_{n;i,j})$, is computed with Equation 3 using the joint probability distribution of the random variables $X_{IDI_{max};n,i,j}$ and $X_{IDI_p;n,i,j}$ (see Equations 2a and 2b),

$$X_{IDI_{max};n,i,j} = \frac{\ln(IDI_{max;n,i,j}) - \ln(IDI_{max;i,j}^{cap,BP_n})}{\sqrt{\beta_{IDI_{max;n,i,j}}^2 + \beta_{IDI_{max;i,j}}^{cap,BP_n}^2}}$$
(2a)

$$X_{IDI_{p};n,i,j} = \frac{\ln(IDI_{p;n,i,j}) - \ln(IDI_{p;i,j}^{cap,BP_n})}{\sqrt{\beta_{IDI_{p;n,i,j}}^2 + \beta_{IDI_{p;i,j}^{cap,BP_n}}^2}}$$
(2b)

$$P_f(BP_{n;i,j}) = 1 - \Phi_2\left(\bar{X}_{IDI_{max};n,i,j}, \bar{X}_{IDI_p;n,i,j}, \rho_{IDI_{max},IDI_p;n,i,j}\right)$$
(3)

where $IDI_{max;n,i,j}$ and $IDI_{max;i,j}^{cap,BP_n}$ are the demand and capacity variables for IDI_{max} , $IDI_{p;n,i,j}$ and $IDI_{p;i,j}^{cap,BP_n}$ are the demand and capacity variables for IDI_p , superimposed bars signify mean values, β represents logarithmic standard deviation, Φ_2 is the bivariate cumulative distribution function, and $\rho_{IDI_{max},IDI_{p};n,i,j}$ is the correlation coefficient between $X_{IDI_{max};n,i,j}$ and $X_{IDI_{p};n,i,j}$. Since the correlation among the random variables representing demands can be estimated from structural analyses, variables $IDI_{max;n;i,j}$ and $IDI_{p;n;i,j}$ are considered to be correlated. There is not sufficient information available about capacity variables $(IDI_{max;i,j}^{cap,BP_n})$ and $IDI_{p;i,j}^{cap,BP_n}$ in the literature to properly model their correlation. Therefore, in this paper, $IDI_{max;i,j}^{cap,BP_n}$ and $IDI_{p;i,j}^{cap,BP_n}$ are considered to be independent. This assumption is a limitation of the joint probability model and requires future studies. Considering that the individual building assessments are based on CS, the terms in Equations 2 and 3 are conditioned on the conditioning building reaching the hazard level associated with the nth BCPO (h_n) using a scenario $(Scen_k)$. For simplicity, the conditional notation is not included in Equations 2 through 3. It is worth noting that the key assumption for Equations 2 and 3 is that the natural logarithm of the EDPs follows a correlated multivariate normal distribution, as described in Appendix G of FEMA P-58-1 (FEMA, 2018a). Unlike FEMA (2018a), Monte Carlo simulation is not used in this methodology to evaluate damage. Instead, integration over the failure/safe domain is used.

The state (failure, not failure) of building i in subarea j for BP_n , evaluated using IDI_{max} and IDI_p independently, is represented by the Bernoulli random variables $Y_{max;n,i,j}$ and $Y_{p;n,i,j}$ (see Equations 4a and 4b), respectively. Therefore, the state of building i in subarea j, $Y_{n,i,j}$, considering both IDI_{max} and IDI_p , can be expressed using the Boolean outcome of $Y_{max;n,i,j}$ and $Y_{p;n,i,j}$ (Equation 5).

$$Y_{max;n,i,j} = \begin{cases} 1 & \text{failure, if } X_{IDI_{max};n,i,j} > 0 \\ 0 & \text{not failure, if } X_{IDI_{max};n,i,j} < 0 \end{cases}$$
(4a)

$$Y_{p;n,i,j} = \begin{cases} 1 & \text{failure, if } X_{IDI_p;n,i,j} > 0 \\ 0 & \text{not failure, if } X_{IDI_p;n,i,j} < 0 \end{cases}$$
(4b)

$$Y_{n,i,j} = \begin{cases} 1 & \text{failure, if } X_{IDI_{max}:n,i,j} > 0 \text{ OR if } X_{IDI_{p};n,i,j} > 0 \\ 0 & \text{not failure, otherwise} \end{cases}$$
 (5)

Conditional assessment of building cluster performance

Building cluster performance is aggregated from the conditional assessments of individual building performance within a building cluster. BCPOs are defined based on the resilience goals for building clusters under a given hazard level (NIST, 2016). Denoting N_b as the total number of spatially distributed buildings in a cluster, the $1 \times N_b$ random vector $\mathbf{Y}_n = \{Y_{n,i,j}\}$ defines the joint state of the buildings for the nth BCPO. Since \mathbf{Y}_n is evaluated using CS, it is dependent on S_a at the fundamental period of the conditioning building i^* in subarea j^* reaching the hazard level h_n associated with the nth BCPO ($s_{a_{h_n},i^*,j^*}$) for a scenario $Scen_k$. Note that the asterisk is used to signify the conditioning building.

Usable floor area is a metric used for individual building resilience assessment (Joyner et al., 2021). In this methodology, the floor area at the community level is considered for building cluster performance assessment. Based on the percentage of the community's floor area failing BP_n , a limit state function $g(Y_n)$ for the nth BCPO is expressed as

$$g(\mathbf{Y}_n) = C_n - \frac{\sum_{i,j} N_{i,j} B_{i,j} A_{i,j} Y_{n,i,j}}{\sum_{i,j} N_{i,j} B_{i,j} A_{i,j}}$$
(6)

where $N_{i,j}$ and $A_{i,j}$ are the number of stories and the floor area per story of building i in subarea j, respectively; $B_{i,j}$ is the number of buildings represented by building i in subarea j; and C_n is the threshold value (between zero and one) defined for the nth BCPO.

The probability of failure for the *n*th *BCPO* of Risk Category II building clusters conditioned on $s_{a_{h_n,i^*,j^*}}$ and $Scen_k$ is evaluated with Equation 7 using the y_n outcomes in the failure domain

 $g(y_n) < 0$. A similar equation can be used for Risk Category IV building clusters. The probability mass function of Y_n conditional on $s_{a_{h_n}i^*,j^*}$ and $Scen_k$, $p_{Y_n}\left(y_n|s_{a_{h_n},i^*,j^*};Scen_k\right)$, is computed using Equation 8 (for simplicity, the conditional notation is not shown),

$$P_{f}\left(BCPO\text{-}II_{n}|s_{a_{h_{n},\,i^{*},\,j^{*}}};Scen_{k}\right) = \sum\nolimits_{a(\mathbf{y_{n}})<0}p_{\mathbf{Y_{n}}}\left(\mathbf{y_{n}}|s_{a_{h_{n},\,i^{*},\,j^{*}}};Scen_{k}\right) \tag{7}$$

$$p_{Y_n}(y_n) = \sum_{y_{n;i,j}} \int_{LL_{i,j}}^{UL_{i,j}} p_{X_n}(x_n) dx_n$$
(8)

where $X_n = \left[\{X_{IDI_{max};n,i,j}\}, \{X_{IDI_p;n,i,j}\} \right]$ is a $1 \times 2N_b$ vector of correlated, standard normal random variables; the lower and upper integration limits (LL and UL) of X_n are selected based on the outcome of $Y_{max;n,i,j}$ and $Y_{p;n,i,j}$ for the variables associated with IDI_{max} and IDI_p , respectively. Note that in Equation 8 the probability content of the $2N_b$ -dimensional continuous variable, X_n , is mapped to the N_b -dimensional discrete variable, Y_n . A multidimensional integration of $p_{X_n}(x_n)$ is used because the safe/failure domain at the building cluster level includes different subsets of safe/failure at the individual building level. The summation on y_n (corresponding to x_n) is used to find the probability of failure for a building considering three possible cases: failure due to IDI_{max} , IDI_p or both.

Building cluster performance assessment

Building cluster performance is evaluated using the building cluster conditional assessments and the total probability theorem. This methodology considers that only one building in the cluster reaches its hazard level h_n ; as such, the conditioning buildings reaching h_n define a set of collectively exhausting, mutually exclusive probabilistic events. The probability of failure of $BCPO-II_n$, $P_f(BCPO-II_n)$, is calculated as

$$P_{f}(BCPO-II_{n}) = \sum_{i^{*}, j^{*}} \left[\sum_{k} P_{f} \left(BCPO-II_{n} | s_{a_{h_{n}, i^{*}, j^{*}}}; Scen_{k} \right) L_{Scen_{k} | h_{n}, i^{*}, j^{*}} \right] L_{h_{n}, i^{*}, j^{*}}$$
(9)

where $L_{Scen_k|h_n,i^*,j^*}$ is the likelihood of scenario $Scen_k$ given that h_n is reached at the conditioning building and L_{h_n,i^*,j^*} is the likelihood of the conditioning building reaching h_n . $L_{Scen_k|h_n,i^*,j^*}$ is considered equal to the contribution of scenario $Scen_k$ to the hazard deaggregation for the S_a at the

fundamental period of the conditioning building. It is assumed that each building has the same likelihood of reaching its hazard level h_n (i.e., L_{h_n, i^*, j^*} is constant for all buildings in the cluster). An equation similar to Equation 9 can be developed for Risk Category IV building clusters.

Earthquake resilience assessment of building clusters considering all hazard levels

The probability of achieving each BCPO (i.e., one minus the corresponding probability of failure) is used to assess the earthquake resilience of the building clusters. The incorporation of BCPO in the definition of building cluster resilience depends on the judgment of the community's decision-makers and stakeholders. This allows for flexibility via assigning the importance of each BCPO to a particular community.

APPLICATION

This methodology is applied to two building clusters across two subareas of San Francisco, CA, to compute the probabilities of failure of three BCPOs for each cluster. The building clusters are residential housing and essential facilities. It is assumed that all buildings in these clusters are designed according to ASCE 7 (ASCE, 2022) as Risk Category II and IV buildings, respectively, with site class CD. As shown in Figure 1, the subareas correspond to the Financial District and the portion of the Mission/Potrero Hill neighborhoods near San Francisco General Hospital. Four representative buildings satisfying ACI 318 (ACI, 2019) reinforced concrete special moment frames requirements are designed and used to represent the buildings in each subarea. Note that this application is for illustration purposes. There is a trade-off between the number of subareas and the computation cost. Obviously, the larger the number of subareas, the more computation cost would be needed, while the accuracy could be increased. The users should balance the computation cost and accuracy based on their requirements and computation resources.

Hazard analysis

After selecting the subareas of interest, hazard analysis is performed to determine the severity of the events defining the hazard levels. Because of the apparent period elongation resulting from the nonlinear behavior of structures and the contribution of higher modes in the structural response, the GM selection is performed to match both the conditional median and logarithmic standard deviation of S_a over a range of periods from 0.2 times the smallest fundamental period to 2 times the largest

fundamental period of the representative buildings in a building cluster in each subarea (NIST, 2011). Building characteristics, which are needed to carry out to perform hazard analysis, the CS, and the GM selection are discussed in the following sections.

Individual building performance

Representative buildings

The four representative buildings that characterize the clusters in each subarea are selected to have 3, 7, 10, and 15 stories. The typical floor plan of the buildings, with the longitudinal axis of the lateral-load-resisting structural system in the horizontal direction, is presented in Figure 2. The story height of the Risk Category II buildings is 4.27 m [14 ft] on the first floor and 3.66 m [12 ft] on the others. For the Risk Category IV buildings, the story height is adjusted such that the clear height per story is identical for both risk categories. Information about the building designs and the pushover analysis results using the building model described below are presented in Table 2. In the pushover analysis, the lateral forces are distributed over the structure's height according to the pattern indicated in the ASCE 7 (ASCE, 2022) equivalent lateral force procedure.

Building model

A 3D model with distributed plasticity was developed for each representative building using OpenSees (McKenna et al., 2010). Nonlinear beam-column elements with sections discretized into concrete core, concrete cover, and steel fibers were used for beams and columns. The modified Kent and Park model was used to account for the confinement effects in the concrete core (Scott et al., 1982). The material model used for the reinforcing steel rebars accounted for a reduction in the compressive stress and strain capacity due to buckling effects (Urmson and Mander, 2012; Sagiroglu and Sasani, 2014), which is dependent on the ratio of the transverse reinforcement clear space to the longitudinal reinforcement diameter. The contribution of the slab to the beam response was considered in the model by using T- and L-beams. The elements' numerical integration was solved using Gauss-Lobatto quadrature. Three and four integration points were used for beam segments and columns, respectively. Additional flexibility due to bar-slip effects was considered by increasing the standard Gauss-Lobatto weight of the elements' integration points at joint faces (Murray et al., 2016) using the expressions presented in NIST (2017). Geometric nonlinearity was considered using the corotational formulation in columns.

Pushover analyses were performed for each structure using the design lateral force pattern. The resulting overstrength ratio (maximum lateral force supported by the structure normalized by the design base shear), Ω , for each representative building is presented in Table 2. In addition, a free vibration simulation starting from the deformed shape associated with the yielding top displacement of the pushover analysis was performed on each model to determine the fundamental period of the structures (Table 2), which was then used for computation of the CS used to estimate S_a in the spatially distributed buildings. It is important to note that the analytical fundamental periods of vibration for the 7-, 10-, and 15-story structures are larger than the approximate periods obtained using ASCE (2022).

Conditional spectra

The spectra for the hazard levels in subareas 1 and 2 for the range of periods for Risk Category II buildings listed in Table 2 are presented in Figure 3. Note that 10 periods were used between the fundamental period of each representative building.

The CS for MCE_R in subareas 1 and 2 conditioned on the fundamental periods of Risk Category II buildings (Table 2) are presented in Figures 4a and 4b, respectively. Although MCE_R spectra in both subareas have the same intensity between 1.0 and 3.0 s (see Figure 3), the CS computed for subareas 1 and 2 are different. This is because the distance of the subareas from the rupture site is not the same for the underlying earthquake scenarios representing the hazard. In contrast, as shown in Figure 4 for deterministic hazards, the four CS in one subarea developed using the conditioning building in another subarea are similar to each other. Because the underlying earthquake scenarios for the same subarea's conditioning buildings and the correlation coefficients among S_a considering spatial correlation are similar. Due to the deaggregation for the same subarea's conditioning buildings, the underlying earthquake scenarios are similar. Considering the distance effect is more significant than the period effect in the correlation, the correlation coefficients are similar. Likewise, for the probabilistic hazards shown in Figure 5, the four CS in one subarea developed using a conditioning building in another subarea are similar to each other. The CS for the design hazard level are developed similarly to those for the extreme deterministic hazard presented in Figure 4.

The CS in subareas 1 and 2 for uniform hazard spectrum associated with a 2475-year mean recurrence interval, an extreme probabilistic hazard level, are presented in Figures 5a and 5b, respectively. Based on the deaggregation for the probabilistic S_a , an earthquake scenario at the San Andreas fault

(Peninsula segment) is the maximum contributor for all conditioning buildings and was used to create the CS in both subareas.

The CS in subareas 1 and 2 for uniform hazard spectrum associated with 2475-year mean recurrence interval (extreme probabilistic hazard level) conditioned on the fundamental period of the Risk Category II 3-story building in subareas 1 and 2 (3st-Sub1-RCII and 3st-Sub2-RCII) for three scenarios are presented in Figures 6a and 6b, respectively. The scenarios are numbered based on their contribution to the hazard deaggregation for the probabilistic S_a at the fundamental period of the conditioning building: the smaller the number, the larger the contribution. Scenario 1 is an earthquake scenario at the San Andreas fault (mentioned above); scenarios 2 and 3 represent ruptures at the Hayward (Northern) and San Gregorio faults, respectively. Despite the similarity of the CS shape for each of the three scenarios, the hazard for each scenario is different. This is because the proportion of having pulse-type GMs increases for the scenarios with larger ε .

Ground motion selection

The GM selection is performed using the procedure described in the methodology section. Mean earthquake scenarios, i.e. mean earthquake magnitudes for each fault, averaging over all of the magnitudes that could occur on each (ASCE, 2022), are obtained from deaggregation. With these mean earthquake scenarios, the resulting earthquake scenarios, even for extreme probabilistic hazard, are reasonably represented with records in the NGA-West2 database (Ancheta et al., 2014). Therefore, the uncertainty associated with earthquakes with a low probability of occurrence (e.g., corresponding to 2500-year mean recurrent interval) is considered in this methodology within the CS calculation by means of ε , the number of log standard deviations between the hazard-consistent intensity measure and the GM prediction equations' median for the mean earthquake scenarios. To represent these mean earthquake scenarios, for subareas 1 and 2, the candidate GMs are selected to have a strike-slip mechanism; rupture to site distance from 0 to 100 km [0 to 62.1 mi]; moment magnitude of [6.5, 8.0] and [6.0, 7.5] for extreme and design hazards, respectively; and Vs₃₀ (average shear wave velocity to a depth of 30 m [\approx 100 ft]) of [213, 640] m/s ([700, 2100] ft/s) corresponding to site classes C, CD, and D. Scale factors between 0.25 and 4 are considered acceptable (Joyner and Sasani, 2020; Joyner et al., 2021; Joyner et al., 2022).

Based on Baker and Lee (2018), an initial GM selection is performed. To further reduce the error between both the natural logarithm of the medians and the log standard deviations of the target CS

(s) and the GM selection suite, an optimization is performed. The error is computed as the sum of errors for several periods within the range from 0.2 times the smallest fundamental period to 2 times the largest fundamental period of the representative buildings in each subarea. The optimization considers replacing one selected GM with one non-selected candidate GM that reduces the error to the maximum extent. The optimization process converges when there is no further reduction in the error. Figures 7 presents the spectra of the 20 GMs selected after optimization in two subareas for MCE_R conditioned on the 3st-Sub1-RCII building. The selected GMs in Figure 7a are "pinned" (i.e., no uncertainty) at the period of the conditioning building in subarea 1. While in Figure 7b, there is uncertainty in S_a at every period for subarea 2 due to the location of conditioning building (in subarea 1).

Engineering demand parameter estimation

The median and logarithmic standard deviation of IDI_{max} and IDI_p computed using the nonlinear time history analysis results are presented in Figures 8 and 9 for Risk Category II and IV buildings, respectively. These values are shown for design, MCE_R (extreme deterministic), and extreme probabilistic (scenarios 1 through 3) hazard levels and correspond to the results for each representative building under the hazard level at its fundamental period. As shown in Figures 8a and 9a, the median IDI_{max} of the representative buildings for the design hazard level is less than or equal to 0.02 and 0.01 for Risk Category II and IV buildings, respectively. These are consistent with the drift limits for which the buildings were designed (ASCE, 2022). The ratio of median IDI_{max} for performance under MCE_R and design hazard levels is approximately 1.57, slightly larger than the ratio for the corresponding spectra of 1.50.

In general, the median IDI_{max} for the 3-story structures is more variable under the extreme probabilistic scenarios, which is due in part to a higher concentration of drift in the first story of these shorter structures (Figures 8a and 9a). For extreme hazards, the median IDI_p for both risk categories is smaller than 0.006 (Figures 8b and 9b). The figures also show that the taller the structure, the larger the IDI_p . β of IDI_p (Figures 8d and 9d) is significantly larger than that of IDI_{max} (Figures 8c and 9c). The variability in the drift response of buildings with different heights (number of stories) in the two subareas and for both risk categories is affected by two factors: that the elastic response spectrum cannot completely capture the nonlinear response of structures and that each building represents only one possible design outcome in terms of section size, variation of strength, and stiffness over height.

The correlation matrix R for the EDP vector (consist of $8 \ IDI_{max}$ and $8 \ IDI_p$ values) in Equation 3 is computed using the nonlinear time history analysis resulted as

$$R = \begin{bmatrix} R_{IDI_{max}} & \overline{R_{IDI_{max}}} & R_{IDI_{max}} & \overline{R_{IDI_{max},IDI_p}} & \overline{R_{IDI_{max},IDI_p}} \\ \dots & R_{IDI_{max}} & \overline{R_{IDI_{max},IDI_p}} & R_{IDI_{max},IDI_p} \\ \dots & \dots & R_{IDI_p} & \overline{R_{IDI_p}} \\ \text{symm.} & \dots & \dots & R_{IDI_p} \end{bmatrix}$$

$$(10)$$

where each submatrix in R is a 4×4 matrix for this application. $R_{IDI_{max}}$ and $R_{IDI_{p}}$ represent the correlation matrices for IDI_{max} and IDI_{p} , respectively. $R_{IDI_{max},IDI_{p}}$ is the cross-correlation between IDI_{max} and IDI_{p} . For these matrices, the correlation is computed from the pool of nonlinear time history analysis outcomes of buildings in the same subarea. However, for the buildings in different subareas, due to the limited information about spatial correlation of EDPs and the different GMs suites across different subareas, the spatial correlation among EDPs is assumed to be equal as the spatial correlation of GM intensity measure. It indicates that the correlation coefficients for EDPs in different subareas are modified by the corresponding spatial correlations of GM intensity measure (shown in Equation 10 with double overbar). Future studies on the spatial correlation among EDPs are needed.

Probabilities associated with performance levels of individual buildings

The probabilities associated with the three performance levels (see Table 1) for individual Risk Category II and IV buildings in subareas 1 and 2 are presented in Figure 10. For ease of comparison with ASCE 7 (ASCE, 2022) performance for MCE_R, the probabilities shown in Figures 10e and 10f are the probabilities of collapse, i.e., the probabilities of failure for collapse prevention performance. As shown in Figure 10a, the probability of functionality for Risk Category II buildings for the design hazard level is approximately 15% to 21%. The corresponding probability for Risk Category IV buildings ranges from 33% to 61% (Figure 10b), which may not be considered a "reasonable probability" range for avoiding damage that prevents the facility from functioning as intended in ASCE 7 (ASCE, 2022). The Risk Category IV buildings' probability of functionality being close to 50% is due to the demand and capacity having approximately the same median, $IDI_{max} = 0.01$ (Figure 9a and Table 1). A reasonable approach to increase the probability of functionality of Risk Category IV buildings is to use enhanced partitions with IDI_{max} capacities larger than 1%.

The probability of safe and usable during repair for Risk Category II buildings for the design and MCE_R hazard level ranges from 63% to 80% and 28% to 37%, respectively (Figure 10c). The corresponding probabilities for Risk Category IV buildings range from 89% to 98% and from 54% to 71% (Figure 10d). These values are comparable with the probabilities of receiving post-earthquake unsafe placards specified in FEMA P-58-5 (FEMA, 2018c). Risk Category II buildings have a 94% and 62% probability of avoiding an unsafe placard based on FEMA P-58-5 (FEMA, 2018c) under design and MCE_R hazard levels, respectively; for Risk Category IV buildings, these probabilities are 99% and 88%, respectively. The probabilities of avoiding an unsafe placard based on FEMA P-58-5 (FEMA, 2018c) are larger than the probabilities for safe and usable during repair calculated in this paper. This is mainly because the limits associated with the unsafe placard used in FEMA P-58-5 (FEMA, 2018c) that IDI_{max} = 3% are larger than those considered in this application – IDI_{max} = 2%.

The ASCE 7 (ASCE, 2022) target probabilities of collapse (structural instability) for the MCE_R hazard are demarcated in Figures 10e and 10f as 10% and 2.5% for Risk Category II and IV buildings, respectively. As shown in Figure 10, all buildings satisfy ASCE target performance except for the 3st-Sub1-RCII building, which has a 10.5% probability of collapse. The difference in the collapse probabilities for different earthquake scenarios is due to the proportion of pulse-type GM records used to characterize the hazard (60% and 45% pulse-type GMs for scenarios 2 and 3, respectively).

Building cluster performance

Building cluster inventory

The inventory of representative buildings in each subarea is presented in Table 3. The building information for the residential housing and essential facilities building clusters is collected from the city of San Francisco's residential building database and critical facilities information, respectively (DataSF, 2020). The seismic performance of these buildings depends on characteristics such as construction material, lateral-load-resisting system, and year of construction. To demonstrate the application of the proposed methodology, however, buildings in each subarea and for both risk categories are classified as a representative building based solely on number of stories. Buildings with upper limits of 4, 8, and 12 stories are assigned to 3-, 7-, and 10-story representative buildings, respectively. Buildings with more than 12 stories are assigned to a representative building with 15 stories. The percentage of the community's floor area per representative building for both clusters is

presented in Figure 11. The largest contributors to the floor area of the residential housing and essential facilities building clusters are 15st-Sub1-RCII and 7st-Sub2-RCIV buildings, respectively.

Building cluster performance objectives

Three BCPOs are proposed based on the publications establishing community resilience goals for short-term recovery phases (e.g., WSEMC, 2012; OSSPAC, 2013; NIST, 2016) and corresponding to building performance levels. The selected resilience metric is the percentage of the total floor area in the building cluster reaches the predefined performance threshold value. BCPOs are independently evaluated for Risk Category II and IV buildings under design, MCE_R (extreme deterministic), and extreme probabilistic (scenarios 1 through 3) hazard levels.

For design hazard level, functionality requirements are different for Risk Category II and IV buildings. As shown in Table 4, the threshold values for BCPO-II₁ and BCPO-IV₁ are set as 30% and 60%, respectively, which allows an evaluation of whether the clusters satisfy the minimum requirement for resuming activities and usual operations following an event (NIST, 2016). The threshold values for BCPO-II₂ and BCPO-IV₂ under design and extreme hazard levels are set as 60%, which can represent the percentage of floor area needed for usual operations (NIST, 2016). BCPO-II₃ and BCPO-IV₃ evaluate the Risk Category II and IV building clusters for collapse (lateral instability) under MCE_R hazard. The corresponding threshold values are set as 10% and 2.5%, which are consistent with ASCE 7 (ASCE, 2022) limits for individual buildings under MCE_R hazard.

Estimation for building cluster (community) performance

Median estimations for building cluster performance are evaluated by aggregating the performance of all buildings (categorized as representative buildings) within the cluster. Using the probability mass function of joint failures for each hazard level (see Equation 8), the median estimations of the percentage of floor area across the building cluster satisfying (or not satisfying) the BCPOs are shown in Figure 12. Note that the conditioning buildings are shown in the horizontal axes of Figure 12. The results are presented for only the hazard levels used in the definition of each BCPO: design hazard for BCPO-II₁, BCPO-II₂, and BCPO-IV₁ and both probabilistic and deterministic extreme hazard for BCPO-II₃, BCPO-IV₂, and BCPO-IV₃ (see Table 4). Since all the median estimations of the percentage of building cluster's floor area collapsing is 0% (i.e., the joint probability of no building collapse is larger than 50%), Figures 12e and 12f present the mean estimations rather than the median

ones. Note that the percentage shown in Figures 12e and 12f refers to the floor area not satisfying the BCPO.

As an example, the results shown in Figure 12b are interpreted as there is a 50% chance of at least 87% and 85% of the building cluster's floor area satisfying BCPO-IV₁ under a design hazard conditioned on a 3- and 7-story building in subarea 2, respectively. This is referred to as a 50% confidence in these building cluster performance estimation. For demonstration purposes, Table 5 provides an example using the 7st-Sub2-RCIV structure as the conditioning building to illustrate how the results in Figure 12b are generated. The percentage of functional building cluster floor area shown in Table 5 is calculated using Figure 11b, that the proportions of 7st-Sub1, 3st-Sub2, and 7st-Sub2 to the community floor area are 7%, 14%, and 79%, respectively. Using the linear interpolation, 85% or more of the building cluster's floor area is expected to remain functional, when the cumulative distribution function reaches 50%. If a different confidence level is preferred, such as 60%, approximately 59% or more of the building cluster's floor area is expected to remain functional.

As shown in Figures 12a, 12c, and 12e, the residential housing building cluster performs better when the conditioning building is in subarea 2, compared to the conditioning building located in subarea 1. This is because 85% of the building cluster's floor area is located in subarea 1 (see Table 3 and Figure 11a) and subjected to a relatively reduced hazard (see Figures 3, 4 and 5). For the essential facilities building cluster, the probability that building cluster's floor area satisfying the BCPOs is larger when the conditioning building is in subarea 1 (see Figures 12b, 12d, and 12f). The reasons are the same as the ones for residual housing building case.

Probability of achieving building cluster performance objectives

The probability of achieving each BCPO is presented in Table 6. For the residential housing building cluster, BCPO-II₁ has a 52% probability to be achieved. Since the difference in the building cluster performances is due to the fact that the buildings are distributed unevenly between the subareas, if more subareas were considered, the probability of achieving BCPO would increase resulted by a more uniform distribution of buildings between the subareas. Based on BCPO-II₂ and BCPO-II₃, the probabilities that the residential housing building cluster can accommodate operations for safe and usable during repair after a design event and satisfy collapse prevention requirements following an extreme event are 80% and 85% (78% for probabilistic extreme), respectively.

Table 6 shows that there is a 72% probability of achieving BCPO-IV₁ (more than 60% functional Risk Category IV buildings). This may not be compliant with the ASCE 7 (ASCE, 2022) expectation that Risk Category IV buildings should remain functional after a design event with a reasonable probability. Furthermore, there is less than a 50% probability that BCPO-IV₂ (more than 60% safe and usable during repair) is satisfied. Again, since these probabilities are affected by uneven distribution of buildings between the subareas, it is expected that the probability of achieving these BCPOs would increase if more subareas were considered and/or the buildings were more evenly distributed. Additionally, the essential facilities building cluster has a 97% probability of meeting BCPO-IV₃ (collapse prevention) under extreme hazard (94% probability for probabilistic extreme). Therefore, the probability of collapse for individual Risk Category IV buildings specified in ASCE 7 (ASCE, 2022) provides a reasonable estimate for building cluster performance.

SUMMARY AND CONCLUSIONS

This paper presents a methodology to evaluate the immediate post-earthquake resilience of building clusters. Compared with the PBEE framework (Deierlein et al., 2003; Moehle and Deierlein, 2004), the methodology in this paper includes the following extensions to assess immediate post-earthquake community resilience:

- The CS considering cross and spatial correlations are used in the hazard analysis to evaluate the hazard intensity in spatially distributed subarea.
- A joint probability model, which accounts for the correlation among EDPs (i.e., IDI_{max} and IDI_{n}), is proposed to estimate the probability of failure of individual building.
- Using a resilience metric that can be evaluated at both individual and building cluster levels (e.g., the usable floor area), BCPOs are defined based on hazard level, target building performance, and building cluster performance threshold value.
- Using the total probability theorem, the probability of the floor area of building cluster achieving BCPOs is quantified by aggregating the conditional assessments of individual building performance.

The earthquake resilience evaluation for the short-term recovery phase is accomplished by discretizing a community area into subareas and assessing the performance of building clusters across those subareas using the total probability theorem. While the BCPOs are defined for two hazard levels

(design and extreme), more hazard levels can readily be included. CS are used to define a hazard level across the community. Three performance objectives are used for both individual buildings and building clusters: functionality, safe and usable during repair, and collapse prevention. Using the aggregation of individual building performances, the building cluster performances are evaluated probabilistically to assess whether the cluster meets specific objectives. The probability of failure for BCPO is evaluated using the failure domain of a limit state function defined in terms of IDI_{max} and IDI_p , and considers the correlation of such building response measures. Using this methodology, the confidence level of achieving each BCPO can be evaluated and compared with a specified target confidence based on the importance of BCPO assigned by the community's decision makers and stakeholders. The achievement of building cluster performance to the community's needs can be determined and provide planning guide to improve the community resilience.

The methodology is demonstrated using two building clusters across two subareas in San Francisco, CA. Buildings within each cluster are categorized by representative 3-, 7-, 10-, and 15-story reinforced concrete special frame structures. It should be emphasized that the values shown in Table 6 and the corresponding discussions about community resilience are obtained based on 1) the two subareas shown in Figure 1, 2) the capacities for building performance levels defined in Table 1, 3) the representative buildings specified in Table 2, 4) the building cluster inventories presented in Table 3, and 5) the BCPOs presented in Table 4. Any changes to these pre-defined parameters/assumptions would affect the results presented in Table 6 and the assessment of community resilience.

Based on the results of the application, the following conclusions are drawn:

 By selecting 20 GMs (pulse-type and ordinary), the median and dispersion of CS can be reasonably represented.

For individual buildings:

- Unlike for Risk Category II structures, the fundamental period of Risk Category IV structures is less than the approximate periods suggested by ASCE (2022). This indicates that such approximate periods may need to be dependent on the Risk Category.
- Collapse prevention performance level for (deterministic) extreme hazard is within the limits
 provided by ASCE (2022) for both Risk Category II and IV structures.

- Under design level hazard, the probabilities of Risk Category II and IV structures being able to remain safe and usable during repair are 62% to 80% and 78% to 90%, respectively. Under deterministic extreme hazard level, these probabilities vary from 30% to 38% and 37% to 53%, respectively.
- Considering the median drift limit capacities used to define building functionality ($IDI_{max} = 1\%$ and $IDI_p = 0.2\%$), the probability of remaining functional for Risk Category IV buildings varies from 33% to 61%, which may not be considered with the expectation from ASCE 7 (ASCE, 2022) that Risk Category IV buildings should remain functional after a design event with a reasonable probability.

For building clusters:

- Collapse prevention performance objectives defined under extreme hazard for both Risk Category II and IV building clusters are achieved with high confidence of 78% to 97%, respectively.
- At the design hazard level, there is a 72% probability that at least 60% of the floor area of the Risk Category IV building cluster remains functional. For the same percentage of the floor to remain safe and usable during repair, this probability drops to 48% and 46% for deterministic and probabilistic extreme hazard levels, respectively.
- To improve the probability of Risk Category IV buildings satisfying functionality at the design hazard level, enhanced nonstructural components with IDI capacities larger than 1% could be used.

Future improvements to this methodology include considering the intermediate and long recovery phases (with recovery time) in BCPOs, evaluating the multivariate joint probability distribution of EDPs, modeling the likelihood of the conditioning building reaching each hazard level, and estimating of correlations among performance level capacities.

DATA AVAILABILITY STATEMENT

Some or all data, models, or code that support the findings of this study are available upon reasonable request from the corresponding author.

ACKNOWLEDGMENTS

This paper is based upon research supported by the National Science Foundation under Grant No. CMMI-2053741. The authors greatly appreciate this support. The first author is also thankful for the support provided by Comexus through the Fulbright-Garcia Robles program.

NOTATION

The following symbols are used in this paper:

 BP_n = Building performance level associated with the *n*th *BCPO*

 $BP_{n;i,j}$ = Building performance level associated with the nth BCPO assessed for building i in subarea j

 h_n = Hazard level associated with the *n*th *BCPO*

 $IDI_{max:n.i.j} = IDI_{max}$ demand on building i in subarea j for the hazard level h_n

 $IDI_{p:n,i,j} = IDI_p$ demand on building i in subarea j for the hazard level h_n

 $IDI_{max;i,j}^{cap,BP_n} = IDI_{max}$ capacity for BP_n of building i in subarea j

 $IDI_{p;i,j}^{cap,BP_n} = IDI_p$ capacity for BP_n of building i in subarea j

 N_b = Total number of spatially distributed buildings in the cluster (sum of buildings across all subareas)

 $s_{a_{h_n,i^*,j^*}} = S_a$ intensity representing hazard level h_n for the conditioning building i^* in subarea j^*

 $X_{IDI_{max};n,i,j}$ = Standardized In demand – In capacity of IDI_{max} for BP_n for the hazard level h_n for building i in subarea j

 $X_{IDI_p;n,i,j}$ = Standardized ln demand – ln capacity of IDI_p for BP_n for the hazard level h_n for building i in subarea j

 $X_n * = 1 \times 2N_b$ continues random vector to calculate the probability of failure of $BP_{n;i,j}$; in this vector, the first and second N_b variables relate to IDI_{max} and IDI_p , respectively

 $Y_{max;n,i,j}$ = State of building i in subarea j for hazard level h_n and BP_n considering only IDI_{max} (by evaluation of $X_{IDI_{max};n,i,j}$)

 $Y_{p;n,i,j}$ = State of building i in subarea j for hazard level h_n and BP_n considering only IDI_p (by evaluation of $X_{IDI_p;n,i,j}$)

 $Y_{n:i,j}$ = State of building i in subarea j for hazard level h_n and BP_n considering IDI_{max} and IDI_p

 $Y_n * = 1 \times N_b$ discrete random vector to define the joint state of buildings for the *n*th *BCPO*

 $\beta_{IDI_{max};n,i,j}$ = Logarithmic standard deviation of IDI_{max} demand on building i in subarea j for the hazard level h_n

 $\beta_{IDI_n;n,i,j}$ = Logarithmic standard deviation of IDI_p demand on building i in subarea j for the hazard level h_n

 $\beta_{IDI_{max}^{cap,BP_n}}$ = Logarithmic standard deviation of IDI_{max} capacity for BP_n of building i in subarea j

 $\beta_{IDI_{n}^{cap,BP_n}}$ = Logarithmic standard deviation of IDI_p capacity for BP_n of building i in subarea j

 $\rho_{IDI_{max},IDI_n;n,i,j}$ = Correlation coefficient between $X_{IDI_{max},n,i,j}$ and $X_{IDI_n;n,i,j}$

For simplicity, the conditional notation on $s_{a_{h_n,i^*,i^*}}$ and $Scen_k$ is not included.

* Vector is shown in bold face.

REFERENCES

ACI, 2019, Building Code Requirements for Structural Concrete, ACI 318-19, American Concrete Institute, Farmington Hills, Missouri.

ASCE, 2022, Minimum Design Loads and Associated Criteria for Buildings and Other Structures, ASCE/SEI 7-22, American Society of Civil Engineers, Reston, Virginia.

ASCE, 2017, Seismic Evaluation and Retrofit of Existing Buildings, ASCE 41-17, American Society of Civil Engineers, Reston, Virginia.

Ancheta, T.D, Darragh, R.B., Stewart, J.P., Seyhan, E., Silva, W.J., Chiou, B.S.J., Wooddell, K.E., Graves, R.W., Kottke, A.R., Boore, D.M., Kishida, T., Donahue, J.L., NGA-West2 database. Earthquake Spectra, 2014. 30(3): 989-1005.

Araya-Letelier, G., Design of building structural systems and enhanced partition walls to improve life cycle costs associated with risk of earthquake damages. Ph.D. dissertation, 2014. Stanford University.

Araya-Letelier, G., Miranda, E., and Deierlein, G., Development and testing of a friction/sliding connection to improve the seismic performance of gypsum partition walls. Earthquake Spectra, 2019. 35(2): 653-677.

Baker, J.W., Conditional Mean Spectrum: Tool for ground motion selection. Journal of Structural Engineering, ASCE, 2011. 137 (3): 322-331.

Baker, J.W., and Jayaram, N., Correlation of spectral acceleration values from NGA ground motion models. Earthquake Spectra, 2008. 21(1): 299-317.

Baker, J.W., and Lee, C., An improved algorithm for selecting ground motions to match a conditional spectrum, Journal of Earthquake Engineering, 2018. 22(4): 708-723.

Baker, J.W., Bradley, B., and Stafford, P., Seismic hazard and risk analysis. 2021. First edition. Cambridge University Press. Cambridge, UK.

Bocchini, P., Christou, V., and Miranda, M., Correlated maps for regional multi-hazard analysis: ideas for a novel approach. In: Multi-hazard approaches to civil infrastructure engineering. 2016. Springer International.

Boore, D., Orientation-independent, nongeometric-mean measures of seismic intensity from two horizontal components of motion. Bulletin of the Seismological Society of America, 2010. 100: 1830-1835.

Bruneau, M., and Reinhorn, A. M., A framework to quantitatively assess and enhance the seismic resilience of communities. Earthquake Spectra, 2003. 19(4): 733-752.

Bruneau, M., and Reinhorn, A. M., Exploring the concept of seismic resilience for acute care facilities. Earthquake Spectra, 2007. 23(1): 41-62.

Burton, H. V., Deierlein, G., Lallemant, D. and Lin, T., Framework for incorporating probabilistic building performance in the assessment of community seismic resilience. Journal of Structural Engineering, 2016. 142(8): C4015007.

Cimellaro, G. P., Reinhorn, A. M., and Bruneau, M., Framework for analytical quantification of disaster resilience. Engineering Structures. 2010. 32(11): 3639-3649.

Cook, D.T., Liel, A.B., Haselton, C.B., Koliou, M.A., A framework for operationalizing the assessment of post-earthquake functional recovery of buildings. Earthquake Spectra, 2022. 38(3): 1972-2007.

DataSF, GSA – City Administrator's Office, Land Use database. 2020. https://data.sfgov.org/Housing-and-Buildings/Land-Use/us3s-fp9q.

Deierlein, G. G., Krawinkler, H., and Cornell, C.A. A framework for performance-based earthquake engineering. In: Proceedings, 7th Pacific Conference on Earthquake Engineering, Paper No. 140. Christchurch, New Zealand: New Zealand Society for Earthquake Engineering, 13-15 February, 2003.

FEMA E-74 Reducing the risks of nonstructural earthquake damage – A practical guide. 2012. Third Edition, prepared by the Applied Technology Council for the Federal Emergency Management Agency, Washington, DC.

FEMA P-58-1 Seismic performance assessment of buildings, Volume 1 – methodology. 2018a. Second Edition, FEMA P-58-1, prepared by the Applied Technology Council for the Federal Emergency Management Agency, Washington, DC.

FEMA P-58-3 Seismic performance assessment of buildings, Volume 3 – supporting electronic materials and background documentation. 2018b. Second Edition, FEMA P-58-3, prepared by the Applied Technology Council for the Federal Emergency Management Agency, Washington, DC.

FEMA P-58-5 Seismic performance assessment of buildings, Volume 5 – expected seismic performance of code-conforming buildings. 2018c. FEMA P-58-5, prepared by the Applied Technology Council for the Federal Emergency Management Agency, Washington, DC.

Goda, K. and Hong, H.P., Spatial correlation of peak ground motions and response spectra. Bulletin of Seismological Society of America, 2008. 98(1): 354-365

Google Earth version 7.1 (January 22, 2022). City of San Francisco, CA, United States of America.

Haselton, C., and Deierlein, G., Assessing seismic collapse safety of modern reinforced concrete moment-frame buildings. Pacific Earthquake Research Center. 2008. PEER report 2007/08.

Haselton, C., Liel, A., Deierlein, G., Dean, B., and Chou, J., Seismic collapse of reinforced concrete buildings. I: Assessment of ductile moment frames, Journal of Structural Engineering, ASCE, 2011. 137(4): 481-491.

Heresi, P., and Miranda, E. Uncertainty in intraevent spatial correlation of elastic pseudo-acceleration spectral ordinates. Bulletin of Earthquake Engineering, 2019. 17(3): 1099-1115.

Heresi, P., and Miranda, E. RPBEE: Performance-based earthquake engineering on a regional scale. Earthquake Spectra, 2023, 39(3): 1328-1351.

Jayaram, N., and Baker, J.W. Correlation model for spatially distributed ground-motion intensities. Earthquake Engineering & Structural Dynamics, 2009. 38(15): 1687-1708.

Joyner, M., and Sasani, M., A multihazard risk-based resilience analysis of east and west coast buildings designed to current codes. Journal of Structural Engineering, ASCE, 2018. 144(9): 1-16.

Joyner, M., and Sasani, M., Building performance for earthquake resilience. Engineering Structures, 2020. 210: 1-14.

Joyner, M., Gardner, C., Puentes, B., and Sasani, M., Resilience-based seismic design of buildings through multiobjective optimization. Engineering Structures, 2021. 246: 1-16.

Joyner, M., Puentes, B., Gardner, C., Steinberg, S., and Sasani, M., Multiobjective optimization of building seismic design for resilience. Journal of Structural Engineering, ASCE, 2022. 148 (4): 04022006.

Koliou, M., van de Lindt, J.W., McAllister, T. P., Ellingwood, B. R., Dillard, M., and Cutler, H., State of the research in community resilience: progress and challenges. Sustainable and Resilient Infrastructure, 2020. 5(3): 131-151.

Lin, P., Wang, N., and Ellingwood, B.R., A risk de-aggregation framework that relates community resilience goals to building performance objectives. Sustainable and Resilient Infrastructure, 2016. 1(1-2): 1-13.

Lin, P. and Wang, N., Stochastic post-disaster functionality recovery of community building portfolios I: Modeling. Structural Safety, 2017. 69: 96-105.

Lin, T., Harmsen, S.C., Baker, J.W., and Luco, N., Conditional spectrum computation incorporating multiple causal earthquakes and ground motion prediction models. Bulletin of the Seismological Society of America, 2013. 103(2A): 1103-1116.

Lin, T., and Baker, J.W., Conditional spectra, Encyclopedia of Earthquake Engineering, Beer, M., Kougioumtzoglou, I.A., Patelli, E., and Au, I.S.K. Editors. 2015, Springer Berlin Heidelberg. P. 13p.

Lizundia, B., Gallagher. Lessons from the post-earthquake safety evaluation in the 2010-2011 canterbury, New Zealand earthquakes and implications for updating ATC-20. In: 15th U.S.-Japan

Workshop on the improvement of Structural Engineering and Resiliency. 2015. Kohala Coast, Hawaii.

Markhvida, M., Ceferino, L., and Baker, J.W., Effect of ground motion correlation on regional seismic loss estimation: application to Lima, Peru using a cross-correlated principal component analysis model. 2017. In: Proceedings of 12th Int. Conf. on Structural Safety and Reliability, Vienna, Austria.

McKenna, F., Scott, M.H., and Fenves, G.L., Nonlinear fine-element analysis software architecture using object composition, 2010, Journal of Computing in Civil Engineering, 24(1): 95-107.

Mieler, M., Stojadinovic, B., Budnitz, R., Comerio, M., and Mahin, S., A framework for linking community-resilience goals to specific performance targets for the built environment. Earthquake Spectra. 2015. 31(3): 1267-1283.

Moehle, J.P., and Deierlein, G.G. A framework methodology for performance-based earthquake engineering. In: Proceedings, 13th World Conference on Earthquake Engineering, Paper No. 679. Vancouver, BC, Canada: Canadian Association for Earthquake Engineering, 1-6 August, 2004.

Molina Hutt, C., Vahanvaty, T., Kourehpaz, P., An analytical framework to assess earthquake-indiced downtime and model recovery of buildings. Earthquake Spectra, 2022. 38(2): 1283-1320.

Murray, J.A., Hecht, E., and Sasani, M., Modeling bar slip in nonductile reinforced concrete columns, 2016, Journal of Structural Engineering, 2016. 142(10): 04016085.

NIST Selecting and scaling earthquake ground motions for performing response-history analyses. 2011. Gaithersburg, Maryland.

NIST Community resilience planning guide for buildings and infrastructure systems. 2016: Gaithersburg, Maryland.

NIST Guidelines for nonlinear structural analysis for design of buildings Part IIb – Reinforced concrete moment frames. 2017. Gaithersburg, Maryland.

Nozhati, S., Ellingwood, B., and Mahmoud, H., Understanding community resilience from a PRA perspective using binary decision diagrams. Risk Analysis. 2019.

Oregon Seismic Safety Policy Advisory Commission (OSSPAC). The Oregon Resilience Plan: Reducing Risk and Improving Recovery for the Next Cascadia Earthquake and Tsunami. 2013.

San Francisco Planning and Urban Research Association (SPUR). Defining resilience: What San Francisco needs from its seismic mitigation policies. San Francisco Urban Research Association, 2008. 479, San Francisco, CA.

City of San Francisco. Latitude: 37.74, Longitude: -122.44, Eye alt: 26.37 km. CSUMB SFML, CA OPC, SIO, NOAA, U.S. Navy, NGA, GEBCO.

Sagiroglu, S., and Sasani, M., Progressive collapse-resisting mechanisms of reinforced concrete structures and effects of initial damage locations, Journal of Structural Engineering, 2014. 140(3): 04013073.

Scott, B., Park, R., and Priestley, M. Stress-strain behavior of concrete confined by overlapping hoops at low and high strain rates, Journal of the American Concrete Institute, 1982. 79(2): 13-27.

Structural Engineering Association of California (SEAOC), Performance Based Seismic Engineering of Buildings, Volume I and II. 1995. Sacramento, California.

Terrametrics, 2022. http://www.earth.google.com [June 26, 2022].

Terzic, V., Villanueva, P.K., Saldana, D., Yoo D.Y. Framework for modelling post-earthquake functional recovery of buildings, Engineering Structures, 2021. 246: 113074.

Urmson, C., and Mander, J.B., Local buckling analysis of longitudinal reinforcing bars, Journal of Structural Engineering, 2012. 138(1): 62-71.

Washington State Emergency Management Council (WSEMC): Seismic Safety Committee. Resilient Washington State: A framework for minimizing loss and improving statewide recovery after an earthquake. 2012.

Table 1. Building performance levels and their corresponding drift limits

	Building		Median drift limits		
BP _n performance level		Definition	$IDI_{max} \ (\%)$	<i>IDI_p</i> (%)	β
n = 1	Functionality	These structures incur minor damage and continue to be fully operational without interruption.	1.0	0.2	0.3
n = 2	Safe and usable during repair	These structures experience moderate damage in structural and nonstructural components leading to a functionality loss.	2.0	0.5	0.3
n = 3	Collapse prevention	These structures meet minimum safety goals but remain closed until they are repaired.	8.5, 7.0, 7.0, 6.5*	N.A.	0.6

^{* 3-, 7-, 10-,} and 15-story representative buildings are defined in the application section.

Table 2. Representative buildings used in the application

Representative building*	Approximate period, used for design (s)	Design base shear kN (kips)	Overstrength ratio	Free-vibration fundamental period (s), used for analysis
3st-Sub1-RCII	0.42	2793 (678)	2.19	0.63
3st-Sub2-RCII	0.42	3221 (724)	2.30	0.63
7st-Sub1&2-RCII	0.88	5369 (1207)	1.93	1.17
10st-Sub1&2-RCII	1.21	6423 (1444)	1.85	1.44
15st-Sub1&2-RCII	1.73	7384 (1660)	1.75	1.81
3st-Sub1-RCIV	0.44	5107 (1148)	2.29	0.53
3st-Sub2-RCIV	0.44	5636 (1267)	2.28	0.50
7st-Sub1&2-RCIV	0.93	9831 (2210)	1.93	0.81
10st-Sub1&2-RCIV	1.26	11450 (2574)	1.86	1.09
15st-Sub1&2-RCIV	1.81	13362 (3004)	1.63	1.52

^{*}Buildings are identified by number of stories – subarea – risk category.

Table 3. Building inventory by subarea

Representative building	Sub	area 1	Subarea 2		
	Number of buildings	Average area per building, m ² (ft ²)	Number of buildings	Average area per building, m ² (ft ²)	
3st-RCII	183	560 (6030)	1955	110 (1181)	
7st-RCII	72	1143 (12310)	5	2025 (21796)	
10st-RCII	35	1788 (19236)	0	0	
15st-RCII	82	1867 (20100)	0	0	
3st-RCIV	0	0	4	2213 (23825)	
7st-RCIV	2	965 (10390)	10	2118 (22796)	

Table 4. Building cluster performance objectives

Building	Risk Category	Hazard level*				
cluster		Design		Extreme		
Residential housing	II	BCPO-II ₁ : BCPO-II ₂ :	More than 30% is functional More than 60% is safe and usable during repair	BCPO-II ₃ :	Less than 10% is likely to collapse (lateral instability)	
Essential IV facilities		BCPO-IV ₁ :	More than 60% is functional	BCPO-IV ₂ : BCPO-IV ₃ :	More than 60% is safe and usable during repair Less than 2.5% is likely to collapse (lateral instability)	

^{*} Percentages are related to the total floor area in the building cluster.

Table 5. probability mass function and cumulative distribution function of floor area of Risk Category IV buildings remaining functional under design hazard conditioned on the 7-story Risk Category IV structure in subarea 2 (7st-Sub2-RCIV)

Building functional state*			Probability mass	Cumulative distribution	Functional building
7st-Sub1	3st-Sub2	7st-Sub2	function (%)	function (%)	cluster floor area (%)
F	F	F	32.5	32.5	100
NF	F	F	5.8	38.3	93
F	NF	F	11.5	49.7	86
NF	NF	F	2.6	52.3	79
F	F	NF	22.9	75.2	21
NF	F	NF	5.9	81.0	14
F	NF	NF	14.4	95.4	7
NF	NF	NF	4.6	100.0	0

^{*} F = functional; NF = nonfunctional.

Table 6. Probability of achieving the building cluster performance objectives

ВСРО	Building cluster	Risk Category	Performance Objective* Hazard level		Probability of achieving BCPO (%)
II ₁			More than 30% is functional	Design	52
II_2	Residential housing	II	More than 60% is safe and usable during repair	Design	80
II3	nousing		Less than 10% is likely to collapse (lateral instability)	Deterministic Extreme	85
				Probabilistic Extreme	78
IV_1			More than 60% is functional	Design	72
IV ₂	Essential facilities	IV	More than 60% is safe and usable during repair	Deterministic Extreme	48
				Probabilistic Extreme	46
			Less than 2.5% is likely to collapse (lateral instability)	Deterministic Extreme	97
				Probabilistic Extreme	94

^{*} Percentages are related to the total floor area in the building cluster.

Figure 1. Two subareas used in this application subarea 1: Financial District; subarea 2: Mission/Potrero Hill (Google Earth, 2024; Terrametrics, 2024; Airbus 2024; CSUMB SFML; CA OPC)

Figure 2. Typical floor plan of the representative buildings (dimensions of columns and beams depend on the representative building)

Figure 3. Spectra for the hazard levels in subareas 1 and 2 for the period range of the Risk Category II buildings

Figure 4. CS for MCER conditioned on Risk Category II buildings (a) subarea 1 and (b) subarea 2 (CS for conditioning buildings outside the subarea of analysis are similar in shape and intensity)

Figure 5. CS for uniform hazard spectrum (UHS) associated with 2475-year mean recurrence interval (extreme probabilistic hazard level) conditioned on Risk Category II buildings (a) subarea 1 and (b) subarea 2 (CS for conditioning buildings outside the subarea of analysis are similar in shape and intensity)

Figure 6. CS for uniform hazard spectrum (UHS) associated with 2475-year mean recurrence interval (extreme probabilistic hazard level) for three earthquake scenarios (a) subarea 1 conditioned on the fundamental period of 3st-Sub1-RCII and (b) subarea 2 conditioned on the fundamental period 3st-Sub2-RCII

Figure 7. GM selection for CS for MCE_R (extreme deterministic hazard level) conditioned on 3st-Sub1-RCII (a) subarea 1 after optimization and (b) subarea 2 after optimization

Figure 8. Median and β of the EDPs for Risk Category II buildings (a) median (%) for IDI_{max} , (b) median (%) for IDI_p , (c) β for IDI_{max} , and (d) β for IDI_p

Figure 9. Median and β of the EDPs for Risk Category IV buildings (a) median (%) for IDI_{max} , (b) median (%) for IDI_p , (c) β for IDI_{max} , and (d) β for IDI_p

Figure 10. Probabilities associated with the three performance levels for individual building in subareas 1 and 2 (a, c, e) Risk Category II and (b, d, f) Risk Category IV 2

Figure 11. Percentage of the community's floor area per representative building (a) residential housing cluster (Risk Category II) and (b) essential facilities cluster (Risk Category IV)

Figure 12. Median (a, b, c, d) and mean (e, f) estimations for the community's total building cluster floor area associated with (a, c, e) BCPO-II₁, BCPO-II₂, and BCPO-II₃ and (b, d, f) BCPO-IV₁, BCPO-IV₂, and BCPO-IV₃



Figure 1. Two subareas used in this application subarea 1: Financial District; subarea 2: Mission/Potrero Hill (Google Earth, 2024; Terrametrics, 2024; CSUMB SFML, CA OPC)

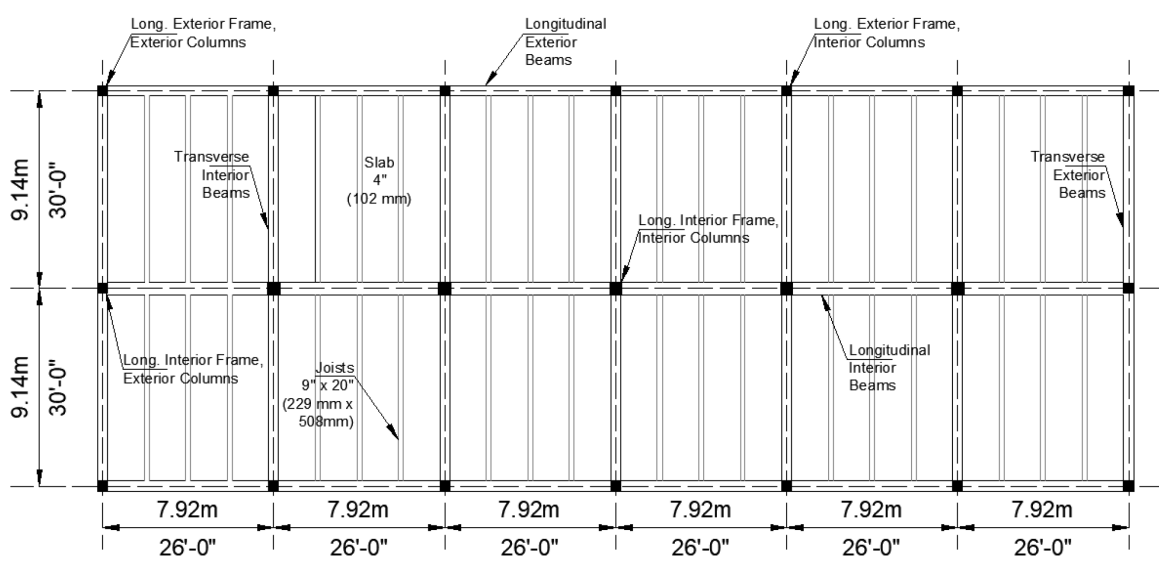


Figure 2. Typical floor plan of the representative buildings (dimensions of columns and beams depend on the representative building)

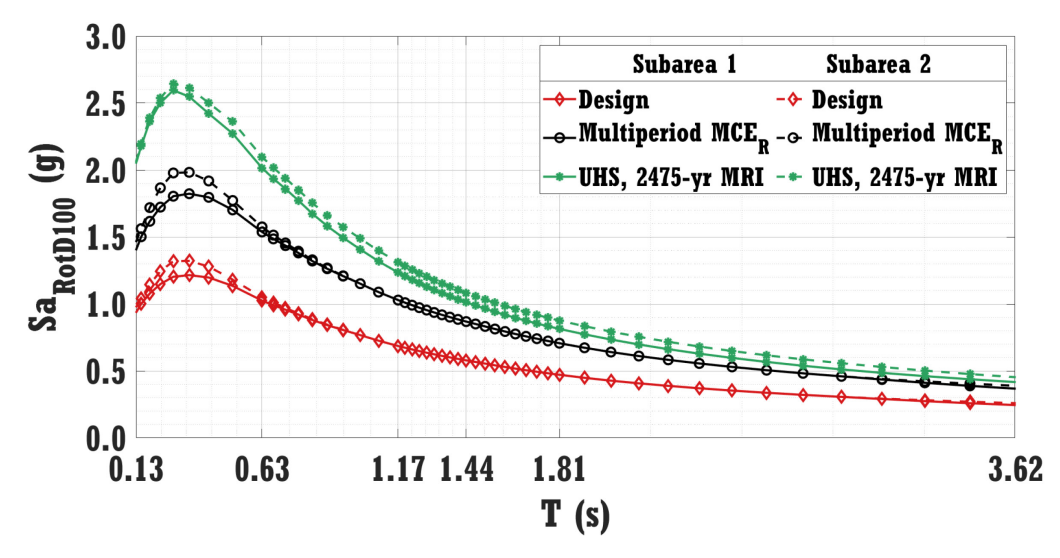


Figure 3. Spectra for the hazard levels in subareas 1 and 2 for the period range of the Risk Category II buildings

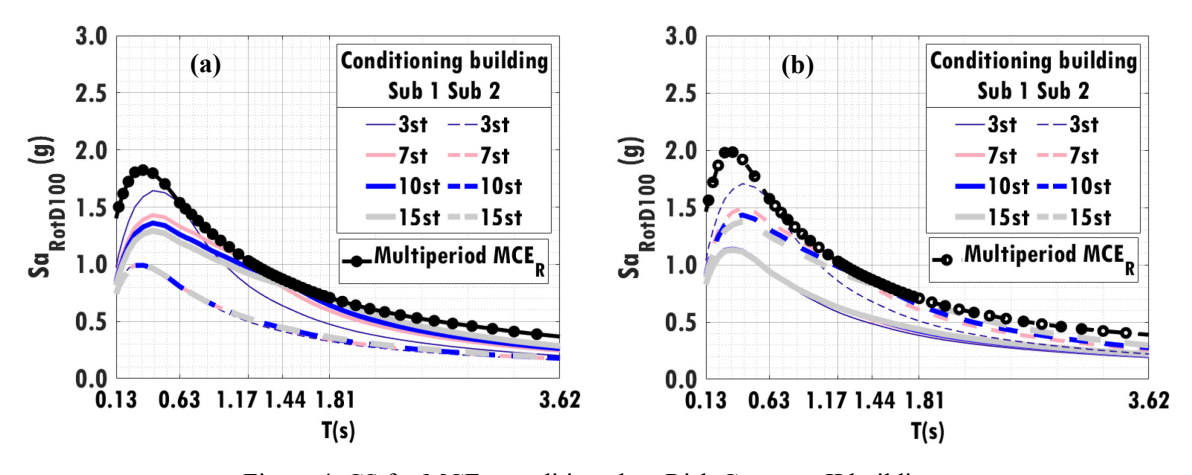


Figure 4. CS for MCE_R conditioned on Risk Category II buildings a) subarea 1; b) subarea 2

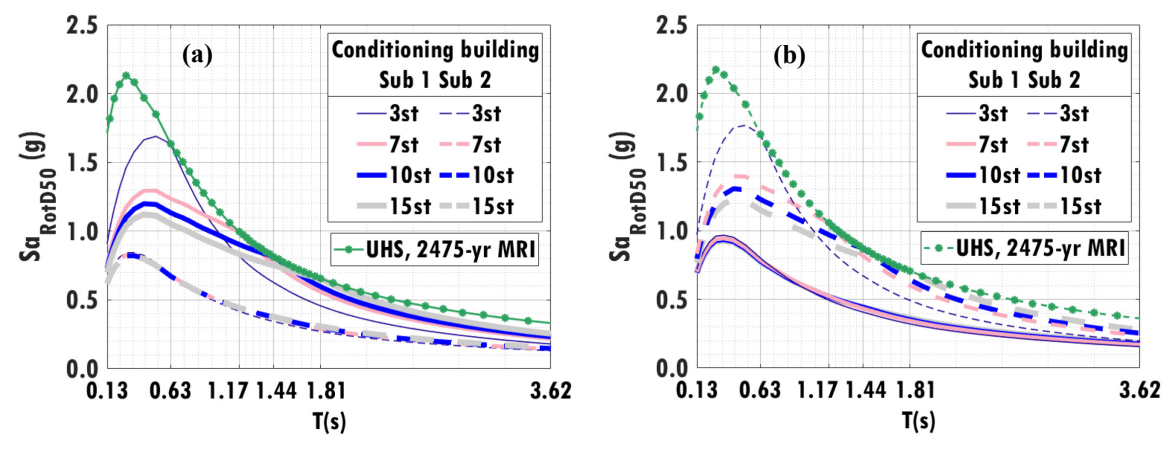


Figure 5. CS for uniform hazard spectrum (UHS) associated with 2475-year mean recurrence interval (extreme probabilistic hazard level) conditioned on Risk Category II buildings a) subarea 1; b) subarea 2 (CS for conditioning buildings outside the subarea of analysis are similar in shape and intensity)

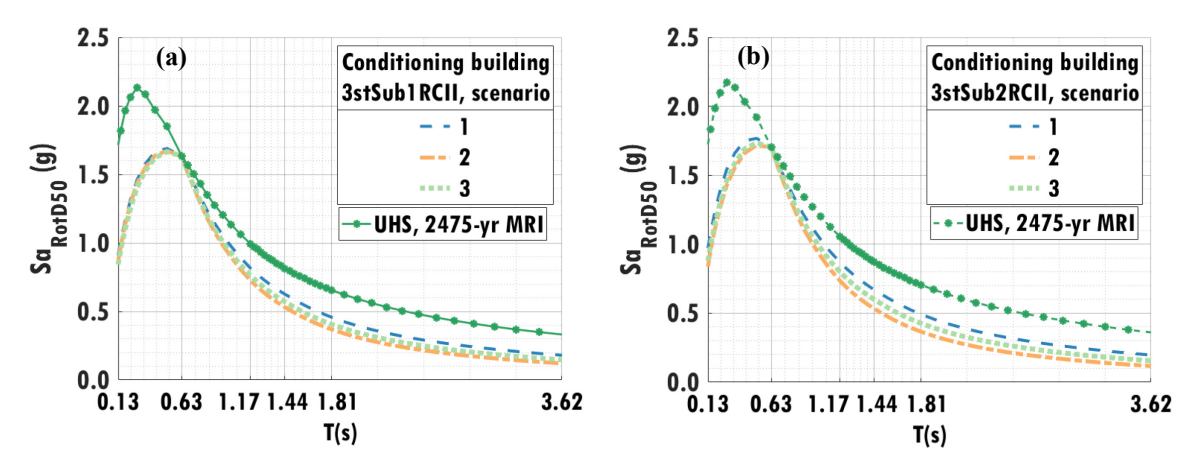


Figure 6. CS for uniform hazard spectrum (UHS) associated with 2475-year mean recurrence interval (extreme probabilistic hazard level) for three earthquake scenarios a) subarea 1, conditioned on the fundamental period of 3st-Sub1-RCII; b) subarea 2, conditioned on the fundamental period 3st-Sub2-RCII

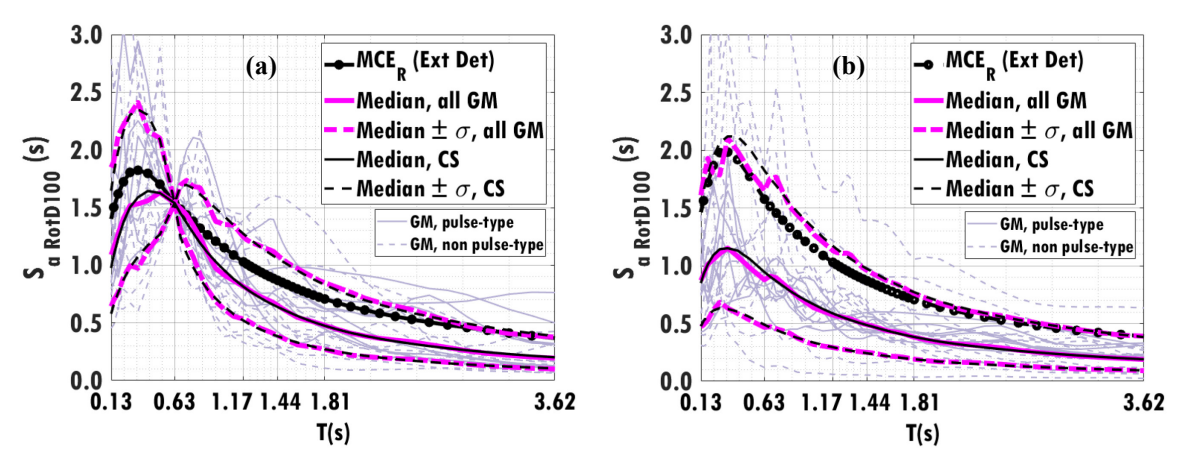


Figure 7. GM selection for CS for MCE_R (extreme deterministic hazard level) conditioned on 3st-Sub1-RCII, a) subarea 1 after optimization; b) subarea 2 after optimization

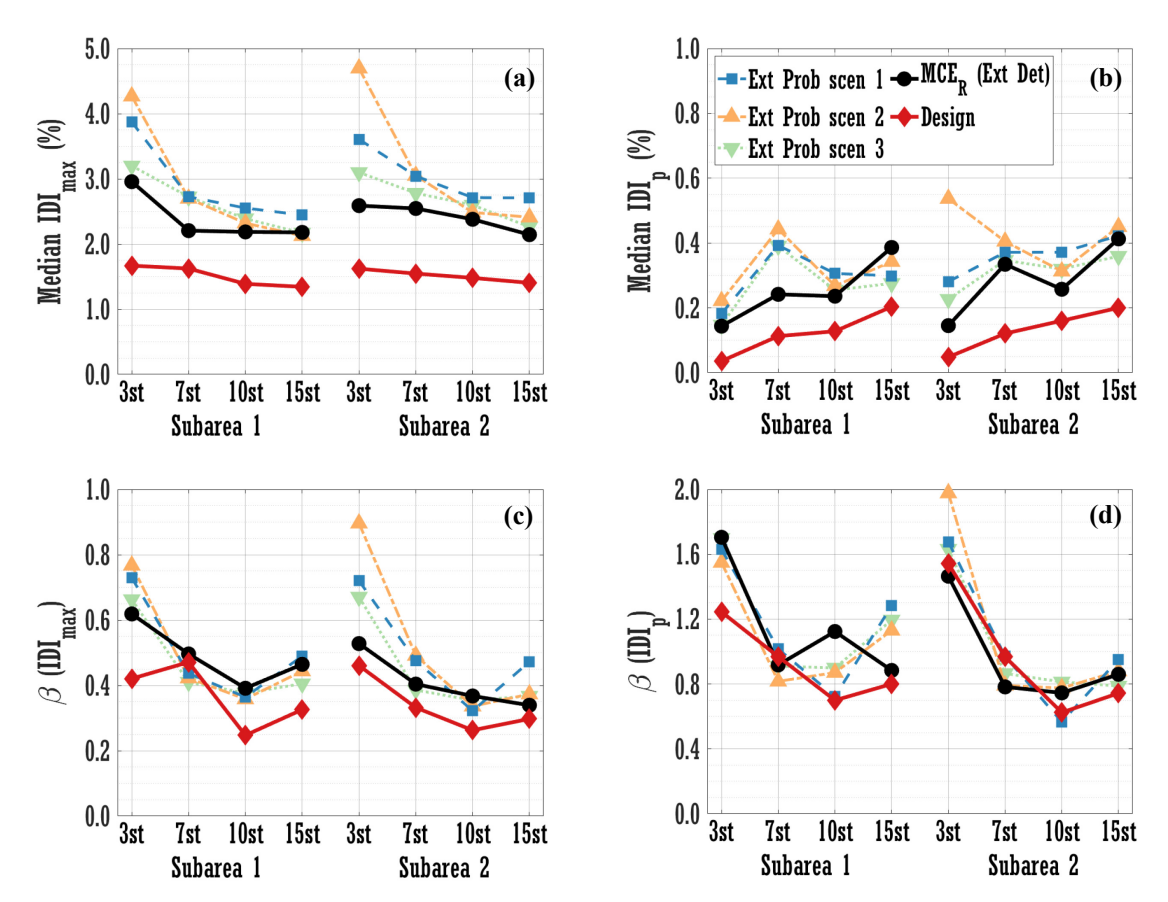


Figure 8. Median and β of the EDPs for Risk Category II buildings, a) median (%) for IDI_{max} ; b) median (%) for IDI_p ; c) β for IDI_{max} ; d) β for IDI_p

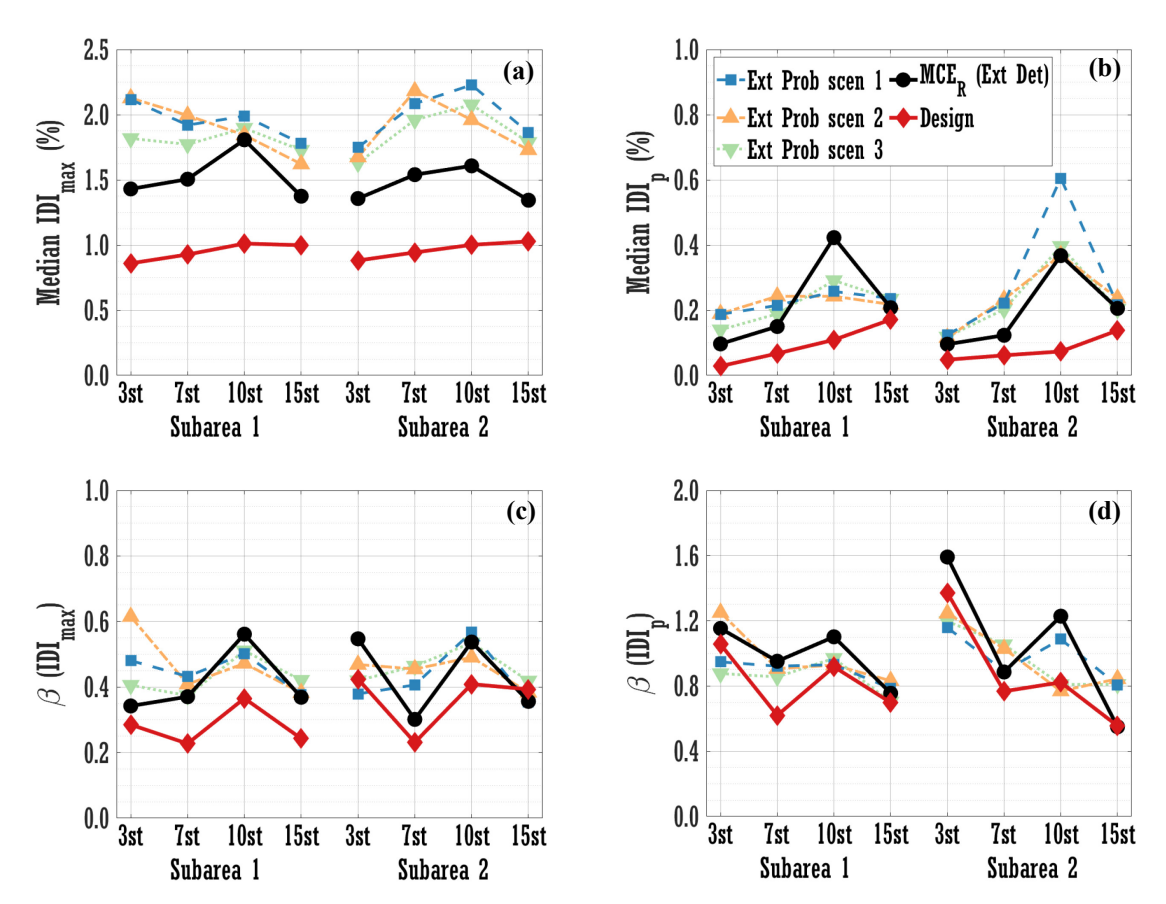


Figure 9. Median and β of the EDPs for Risk Category IV buildings, a) median (%) for IDI_{max} ; b) median (%) for IDI_p ; c) β for IDI_{max} ; d) β for IDI_p

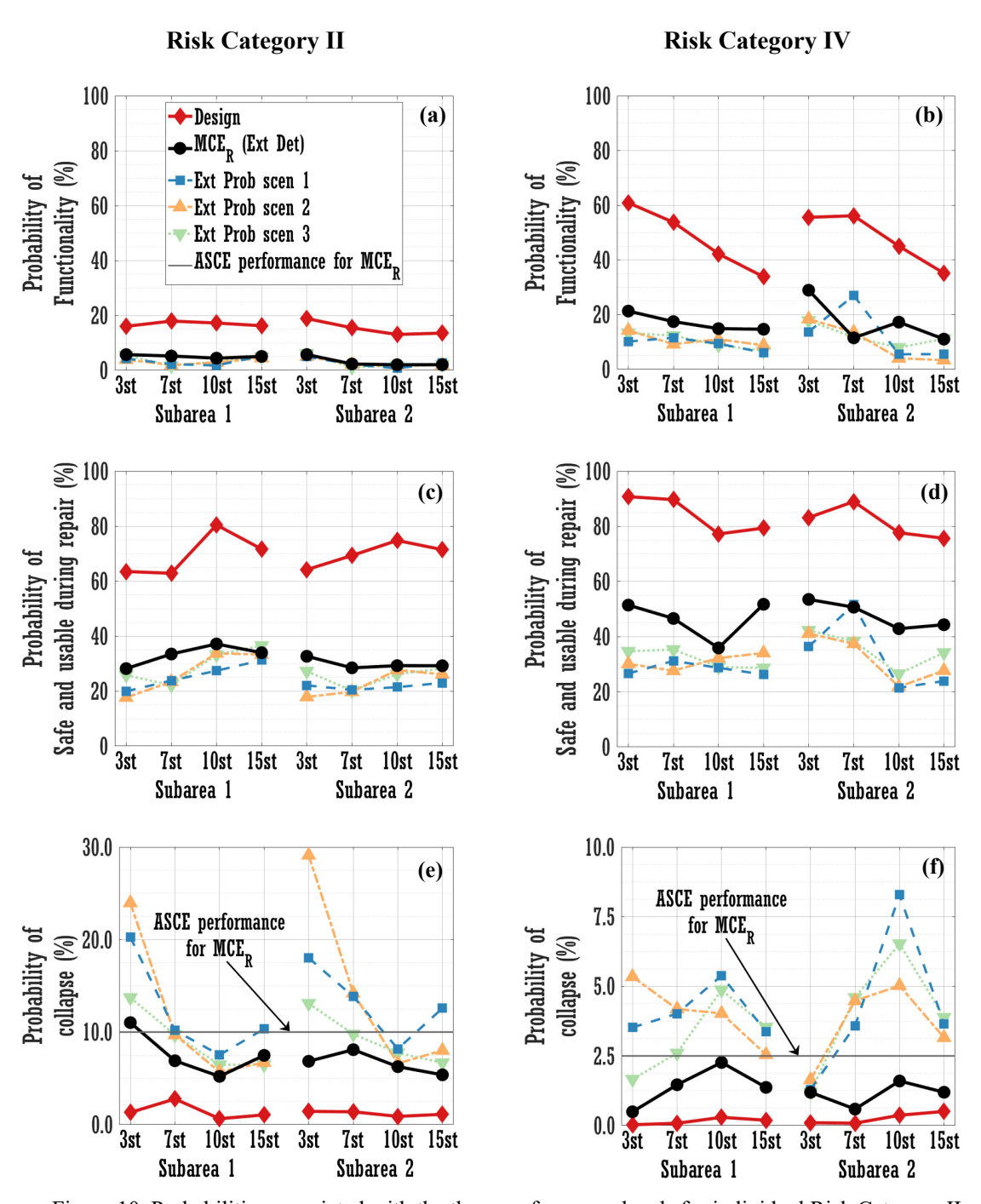


Figure 10. Probabilities associated with the three performance levels for individual Risk Category II (a,c,e) and IV (b,d,f) buildings in subareas 1 and 2

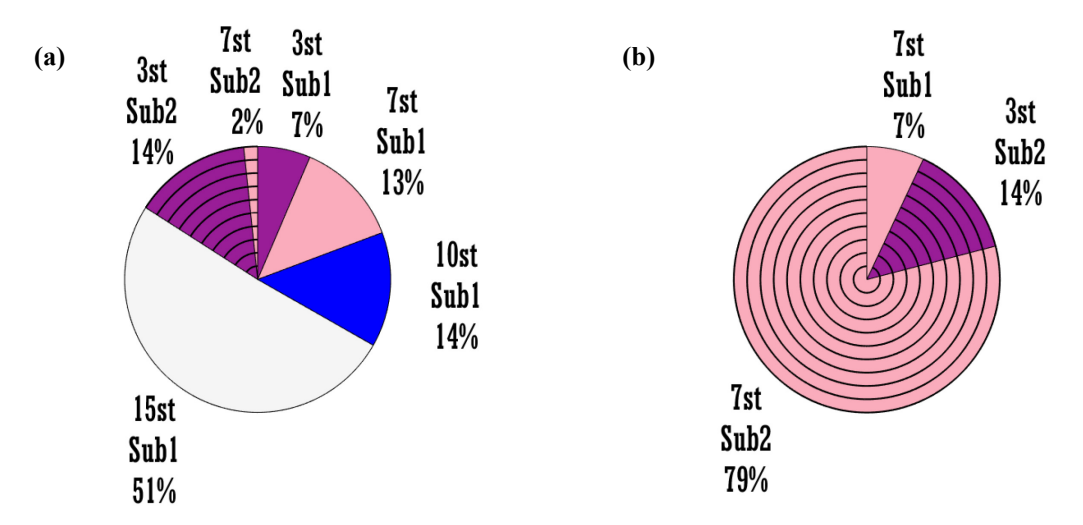


Figure 11. Percentage of the community's floor area per representative building, a) residential housing cluster (Risk Category II); b) essential facilities cluster (Risk Category IV)

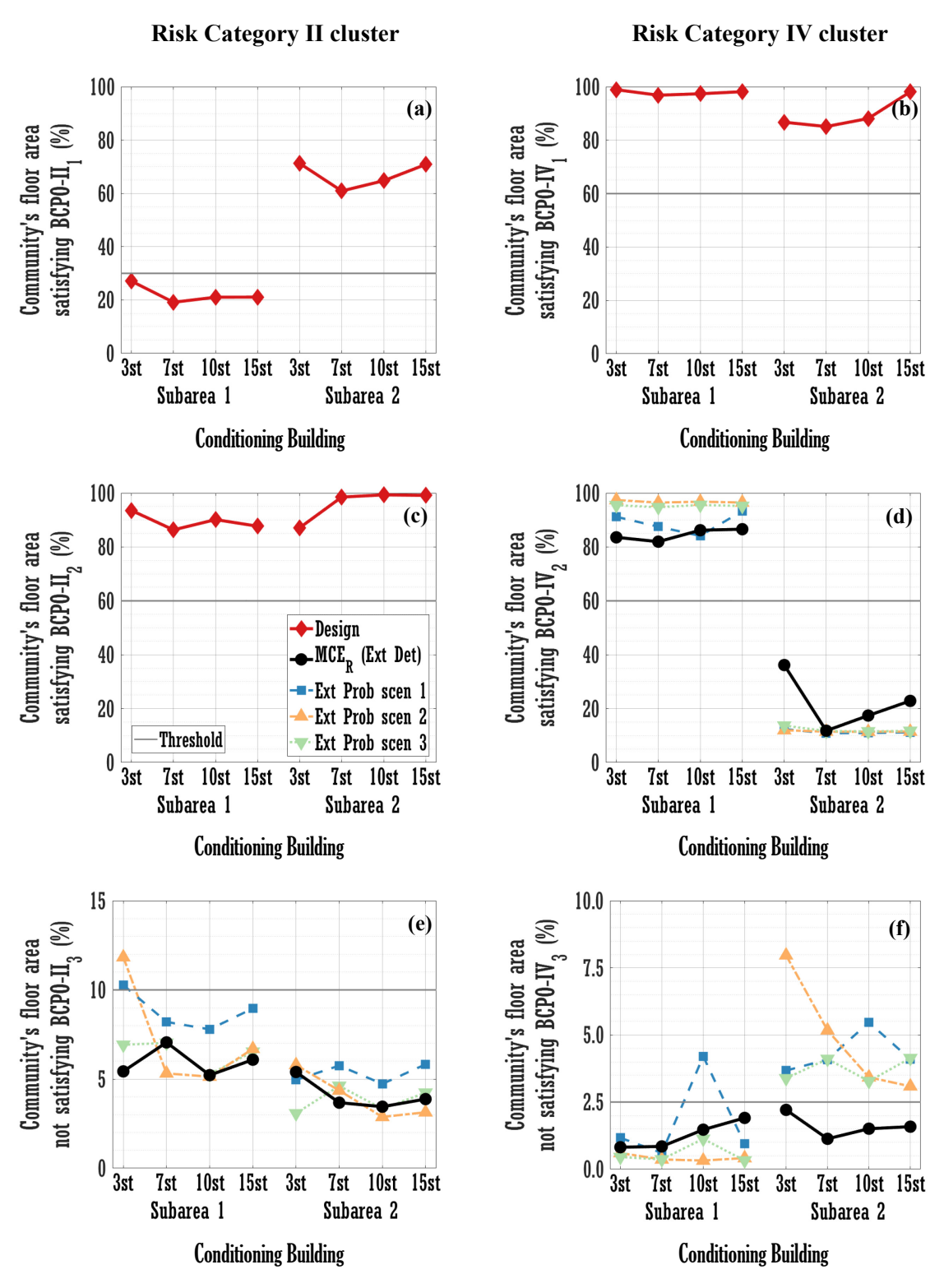


Figure 12. Median (a, b, c, d) and mean (e, f) estimations of the community's total building cluster floor area associated with BCPO-II₁, -II₂, and -II₃ (a, c, e) and BCPO-IV₁, -IV₂, and -IV₃ (b, d, f) BCPO-IV₁, BCPO-IV₂, and BCPO-IV₃